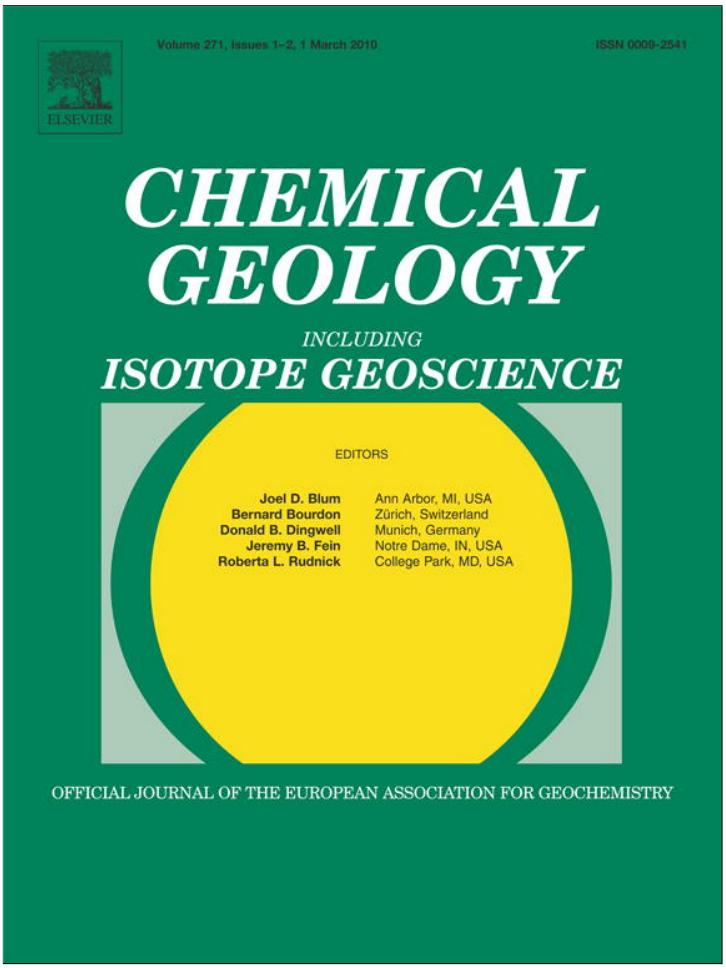

Chemical Geology 271 (2010) 44–51

Contents lists available at ScienceDirect

Chemical Geology

journal homepage: www.elsevier.com/locate/chemgeo

Investigating the geochemical impact of burrowing animals: Proton and cadmium adsorption onto the mucus lining of *Terebellid* polychaete worms

S.V. Lalonde *, L.T. Dafoe, S.G. Pemberton, M.K. Gingras, K.O. Konhauser

Department of Earth and Atmospheric Sciences, 1-26 Earth Sciences Building, University of Alberta, Edmonton, AB, Canada

ARTICLE INFO

Article history:
Received 3 June 2009
Received in revised form 10 December 2009
Accepted 10 December 2009

Editor: J. Fein

Keywords:
Polychaete worms
Burrows
Mucous
Metal adsorption

ABSTRACT

Sediment–water interfaces are the sites of intense chemical activity in natural systems. Burrowing animals extend this interface, and at times coat it with mucous materials they secrete to line their burrows. However, the chemical reactivity of these burrow linings is poorly understood. In this study, we incubated burrowing terebellid worms (*Thelepus crispus*) for the purposes of harvesting their mucus secretions and investigating its composition and metal adsorptive properties. The mucus was comprised of proteins, carbohydrates, and lipids in an approximate ratio of 200:50:1, and FTIR spectroscopy revealed abundant carboxyl, phosphoryl, hydroxyl, amino, and thiol functional groups typical of mucin-like material. Potentiometric titration data were best fit by a three-site surface complexation model, with a total ligand density of 11.26 ± 1.79 mmol per dry gram, which is relatively high compared to previously-studied humic substances and microbial biomass. Cd adsorption experiments demonstrated that the two most acidic ligands, inferred to represent carboxyl and phosphoryl functional groups, respectively, possessed cadmium stability constants that were comparable to analogous ligands inferred for bacterial surfaces. The third ligand, however, differed from bacterial surfaces in that it likely represents thiol functional groups, and displayed a higher Cd stability constant commensurate with the chalcophile nature of organic sulfur ligands. These results indicate that mucous burrow linings such as those produced by terebellid worms are geochemically important for driving metal adsorption and mineral nucleation reactions at the burrow–water interface.

1. Introduction

Estuaries are the depositional interface between fluvial- and marine-waters. Estuarine settings are also widely regarded as sediment sinks that trap land-derived detritus and tidally delivered sands. Concomitant with sediment transport is the arrival of dissolved ions from fluvial and marine water sources. The juxtaposition of fine-grained sediments (i.e. silts and clays), metal ions, and rapid changes in water temperature, salinity, and chemistry due to mixing, leads to the accumulation of metals at the seafloor. The amount of accumulated metals will depend on several processes, including: (1) the composition of the sediment; (2) transport of metals from the bulk ocean water to sediment porewaters; (3) transformation of metals (e.g. methylation, hydrolysis, oxidation–reduction); (4) competition between sediment minerals and organic phases for metals; and (5) the influence of bioturbation on these processes (Bryan and Langston, 1992).

The distribution of metals in estuarine settings is reasonably well studied. This is due to a number of reasons, including the economic use of estuaries for shellfish harvesting (e.g. Willapa Bay, Chesapeake Bay, Prince Edward Island) and the common occurrence of industry along fluvial inputs to estuaries (e.g. Chiffoleau et al., 1994; Millward and Glegg, 1997; Benoit et al., 1994). Traditionally, studies have focused on the partitioning of metals into fine-grained sediment and on the enrichment of metals in animals resulting from bioaccumulation (e.g. Bryan and Hummerstone, 1973; Bryan et al., 1983; Luoma et al., 1998). One commonly overlooked component in these types of studies is the presence of organic coatings produced by burrowing organisms that are prevalent along the sediment–water interface.

A variety of worms are known to thrive in estuarine settings, including polychaetes, nemerteans and hemichordates. Indeed, worm-like organisms represent one of the most important group of macroscopic, bioturbating animals in marginal-marine settings; more than 10,000 species of marine polychaetes have been identified in settings ranging from the intertidal through to the continental shelf (Rouse and Fauchald, 1997). Estuarine worms are diverse as well, and are represented by the Subclass Palpata and the families Glyceridae, Nephtyidae, Nereididae, Serpulidae, Sabellidae, Spionidae, Pectinariidae, and Terebellidae. Worms within these families are generally capable of binding sediment with mucous excretions that serve to physically support burrow walls, prevent desiccation, and function as nutrient-rich organic substrates that foster microbial symbiosis within the burrow lining (e.g., Aller and Aller, 1986).

The presence of mucous linings at the sediment–water interface likely plays an important role in ion complexation and mineral

* Corresponding author.
E-mail address: stefan.lalonde@ualberta.ca (S.V. Lalonde).

0009-2541/$ – see front matter © 2009 Elsevier B.V. All rights reserved.
doi:10.1016/j.chemgeo.2009.12.010

nucleation reactions due to the presence of highly reactive surface adsorption sites typical of organic matter. It is well known that the surfaces of organic matter in natural systems, including bacterial, fungal, and eukaryotic cells, as well as natural organic matter (dissolved and particulate phases), possess functional group ligands that are anionic at seawater pH and are capable of binding metal cations and nucleating mineral phases (c.f. Konhauser 2007 and references therein). Certainly, while previous work has demonstrated the association of metals and minerals with burrow linings (Over, 1988; Zorn et al., 2007), a complete understanding of processes influencing the accumulation of metals in estuarine sediments must also include the adsorptive role of macrofaunal mucous material.

In this study, we incubated the terebellid polychaete *Thelepus crispus* for the purposes of isolating its mucous burrow lining for chemical characterization both in terms of composition and surface adsorptive behavior. The latter was assessed by potentiometric titration and Cd adsorption experiments, and the results modeled within a surface complexation framework that permits the extrapolation of our experimentally-derived thermodynamic constants to systems that vary considerably in terms of pH, ionic strength, and temperature. We demonstrate through this approach that metal adsorption onto worm mucus (1) can be accounted for by surface complexation modeling that takes into account adsorptive ligand properties and metal-ligand stability constants and (2) appears to differ from bacterial surfaces and other organic matter by an abundance of highly-chalcophile thiol functional groups.

2. Methods

2.1. Mucus procurement

Thelepus crispus terebellid worms were collected by Westwind sealab supply (Victoria, BC) and stored in cold seawater during overnight shipment to the University of Alberta. Worms were segregated into polycarbonate containers with lids and walls that were perforated by hand drill to promote water circulation, and the containers were submerged in a continuously circulating salt–water tank at 4 to 8 °C for 15 days. Three different substrates were explored for promoting burrow formation: (1) worms were placed on 100 mesh acid-washed quartz sand (Sigma-Aldrich Canada, Oakville, Ontario), (2) worms were individually placed within 15 mm glass test tubes (Fisher Scientific, Ottawa, Ontario), and (3) worms were individually placed within sections of PVC tubing (1/2 inch inner diameter, Fisher Scientific, Ottawa, Ontario) that were sealed at one end with cheesecloth. Only the PVC tubing promoted burrow formation; in each instance, the worm lined the PVC tubing with mucous material, and in some cases, the worm exited the open end of the tubing, extending the burrow well beyond the length of tubing (see Fig. 1). After 15 days, the PVC tubes containing mucous-lined burrows were collected. For each, the PVC tubing was split by sterile scalpel, and the mucous burrow linings were easily separated from the PVC with tweezers. The mucous lining had incorporated within it sand grains, shell fragments and organic matter from the surrounding tank, and brown fecal matter generated by the worms themselves. The mucous material was cleaned vigorously several times by rinsing under a stream of ultrapure water with the use of forceps and spatula to physically remove any detritus not washed away by water. After all the visible foreign matter had been removed, mucous samples were stored in ultrapure water at 4 °C until later use.

2.2. Mucus compositional analysis

Subsamples of mucous material were incubated in 0.01 M HCl for 30 min to remove any carbonate components, rinsed 3 times with ultrapure water, and lyophilized for further analysis. Major element composition (C,H,N,S) was determined using a Carlo Erba EA 1108 elemental analyzer. Weight percent nitrogen was used as an estimate of protein content (crude protein (CP) = N × 6.25) (Maynard and

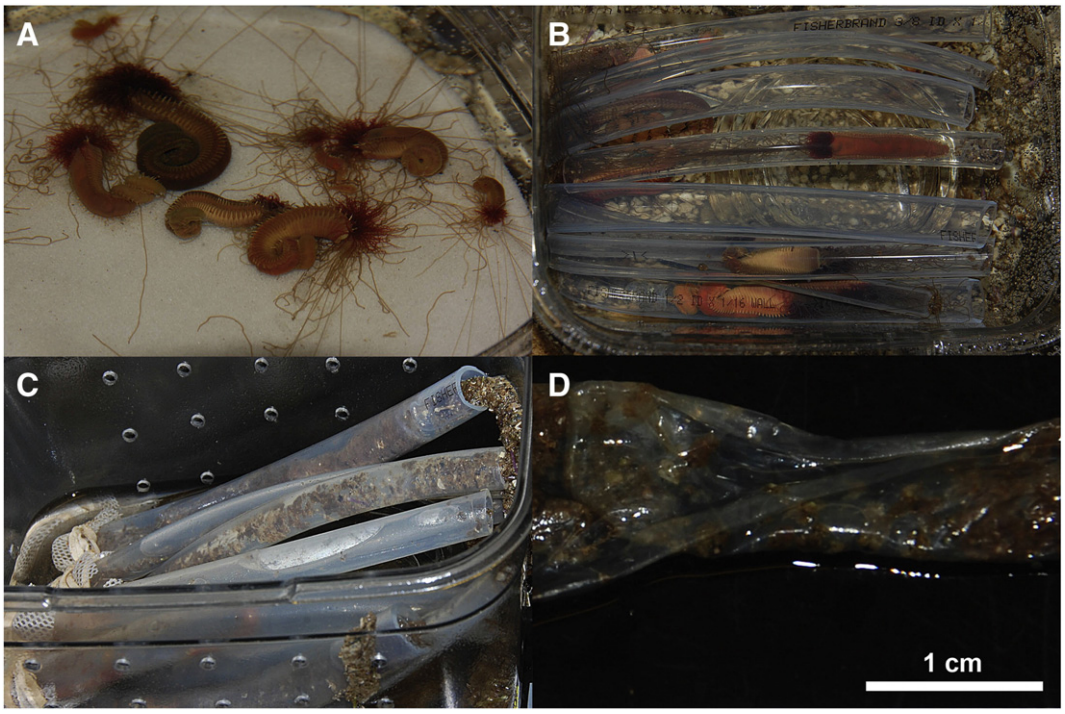

Fig. 1. (A) Terebellid *Thelepus crispus* worms resting on pure quartz sand within an isolated section of a circulating salt–water tank. Note the extended palps used to transport food particles to the mouth. (B) Worms in another isolated section of the same tank, inserted into 1/2 inch PVC tubing to stimulate mucus production. One end of each tube was subsequently sealed with cheesecloth for the duration of incubation. (C) Mucous burrow linings produced after 15 days of incubation in PVC tubing. Several worms continued to produce burrows even upon exiting their PVC tubing. (D) Isolated burrow lining. Brown substance likely represents microbial and fecal organic matter, and was removed by scraping, agitation, and rinsing prior to analyses.

Loosli, 1969). Carbohydrate and fatty acid compositions were determined by solvent extraction on lyophilized samples followed by chromatography at the Human Nutrition Research Unit, University of Alberta. FTIR spectra were collected from 650 to 4000 cm^{-1}, at 0.5 cm^{-1} resolution, using a Nicolet Magna 750 FTIR spectrometer connected to a Nic-plan FTIR microscope operating in absorbance mode. Sixty four scans of air-dried samples on a KCl plate were co-added to obtain the final spectra, with scans of the clean KCl plate prior to mucous addition used for background correction.

2.3. Acid-base titration and Cd adsorption

All glassware and plasticware was acid-washed for >12 h in a 30% v/v HCl bath, rinsed three times with ultrapure water, soaked in an ultrapure water bath for >24 h, rinsed again three times, and dried prior to use. The preparation of all solutions was done gravimetrically on an analytical balance. Mucous material was rinsed three times in ~50 ml of 0.5 M NaCl, resuspended in ~30 ml of 0.5 M NaCl in wide-mouth pyrex beakers (for final mucus concentrations of 0.75–0.9 dry g/L), and acidified to pH~3 with 2 M HCl. A double-junction glass pH electrode (Orion ROSS ultra, filled with 3 M KCl) was calibrated using commercial pH buffers (Thermo Fisher Scientific, Waltham, MA; pH 2, 4, 7, 10, 12) that had been adjusted to 0.5 M NaCl by the addition of NaCl salt, and added to the flask along with a Teflon stir bar, gas bubbler, thermocouple, and titrant dispenser. The flask was then sealed with parafilm and purged with N_2 for thirty minutes prior to titration, and throughout titration. Titrations were performed using a computer-controlled PC-Titrate auto-titrator (Mandel Scientific, Guelph, Ontario) set to deliver 0.01 ± 0.00005 M NaOH (commercial titrant, Thermo Fisher Scientific, Waltham, MA) in increments of 10 additions per pH unit, from pH 3 to 11, with stability criteria of 0.5 mV/s between additions. NaOH titrant was purged for 30 min with N_2 prior to titration, each titration lasted approximately 1 h, with sample temperature remaining approximately constant (23 ± 1 °C) throughout all titrations. Several samples were first acid-washed for 30 min in 0.01 M HCl to remove any carbonate components prior to preparation and titration, although this acid-washing step had no discernable effect (data not shown). After titration, mucous material was filtered onto 1.2 µm Whatman GF/C filters and air-dried to constant mass.

Mucous material for Cd adsorption experiments was washed in 0.5 M NaCl as above, but suspended in a magnetically stirred 0.5 M NaCl solution containing 5 ppm Cd (prepared from a 1000 ppm Cd commercial AAS standard, Fisher Scientific) that had been acidified to pH 2.0–2.5 with 2 M HCl. Due to the limited amount of mucous material available, Cd adsorption experiments were run in a serial fashion, rather than a batch fashion; the adsorption experiments were equilibrated for 30 min, aliquots of ~10 ml were removed by syringe and filtered to 0.22 µm using nylon membrane filters, the pH of the experiment was adjusted up by one pH unit using 2 M NaOH, and the process was repeated until pH~11 was achieved. The adsorption experiments were performed in duplicate, and the results were combined for a single adsorption isotherm. Cd adsorption blanks were not run simultaneously, but have previously indicated negligible adsorption to the experimental apparatus (data not shown). Chemical equilibrium modeling of Cd speciation in experimental solutions was performed using visual MINTEQ (Gustafsson, 2000) with SIT activity correction and stability constants from the MINTEQA2 v4.0 database (Allison et al., 1991).

3. Results and discussion

The *Thelepus* worms (Fig. 1A) generated copious amounts of mucous material when placed in open-ended sections of PVC tubing and submerged in a circulating salt water tank at 4–8 °C for 15 days (Fig. 1B and C). The worms failed to create mucous material when placed on pure quartz sand or in round-bottom glass test tubes (data not shown). In the construction of their mucus-lined PVC domiciles, the worms used their palps to gather material from outside their restricted area of the salt–water tank, and added this material to the mucous matrix.

3.1. Composition of mucous lining

The results of compositional analysis (CHNS, carbohydrates, and lipids) are presented in Table 1. Considering that mucous glycoproteins consist of a protein core to which carbohydrate moieties are attached, the abundance of protein (~20 wt.%) relative to carbohydrate (~5%) is not surprising. Lipids form only a minor constituent of the mucous material. With regards to the elemental analysis, of particular note is the presence of sulfur, which is consistent with the high abundance of thiol-conferring cysteine residues that characterize mucous glycoproteins (Leitner et al., 2003).

FTIR spectra of the mucous material (Fig. 2A) shows a composition consistent with heterogeneous organic matter; strong absorption peaks can be tentatively assigned to C–O stretching, S O stretching, CH_2 scissoring, N–H bending (amide II), N–C O stretching (amide I), and various C–H stretching modes are present at 1070, 1180, 1448, 1543, 1656, and 2851 and 2926 cm^{-1}, respectively (Brandenburg and Seydel, 1996; Bavington et al., 2004). Comparison with FTIR spectra obtained for echinoderm mucous material (e.g., Bavington et al., 2004) reveals striking similarities that likely stem from the well conserved and broadly distributed nature of the mucin family of glycoproteins that appear to dominate these materials (Lang et al., 2007). Of the three echinoderm mucins investigated by Bavington et al. (2004), the FTIR spectra of partially purified mucin from the brittlestar *Ophiocomina nigra* provided a nearly identical match to the terebellid mucous material (Fig. 2B, reproduced from Bavington et al. (2004)). Spectra representing two other echinoderm species, *M. glacialis* and *P. pulvillus*, as well as spectra for bovine mucin, porcine mucin, bovine aggrecan, heparin, chondroitin-4-sulfate, dermatan sulfate, and hyaluronic acid all show adsorption features that are broadly consistent with the terebellid mucus, as well as with each other, highlighting the common organic functional groups comprising these diverse mucin-type glycoproteins (Bavington et al., 2004). This commonality is not surprising considering that mucin-type glycoproteins are widely-occurring biomolecules whose relatively ancient origins can be traced to as far as lower metazoa (e.g., sea anemones; Lang et al., 2007).

3.2. Proton adsorption and discrete ligand modeling

Potentiometric titration data is first evaluated as charge excess in the titration system, expressed at any point in the titration as

$$C_b+[H^+]+[ANC]=C_a+[OH^-]+\sum_{j=1}^{n}[L_j^-] \quad (1)$$

where C_b and C_a are the concentrations of base and acid, $[H^+]$ and $[OH^-]$ are concentrations calculated with SIT activity coefficients (Pettit et al., 2006) from H^+ activity data recorded by the pH electrode, $[L_j^-]$ is the concentration of deprotonated functional groups for the *j*th monoprotic ligand of *n* possible ligands, and the acid-neutralizing capacity [ANC] is a constant representing the difference between functional groups that remain protonated and

Table 1
Terebellid mucous compositional data. All data expressed in weight percent (error 2SE).
*Single analysis.

Carbon	Hydrogen	Nitrogen	Sulfur	Protein	Carbohydrarte	Lipid*
15.70 ± 1.64	2.37 ± 0.35	3.13 ± 0.41	1.23 ± 0.08	19.56 ± 4.54	4.72 ± 1.21	0.10

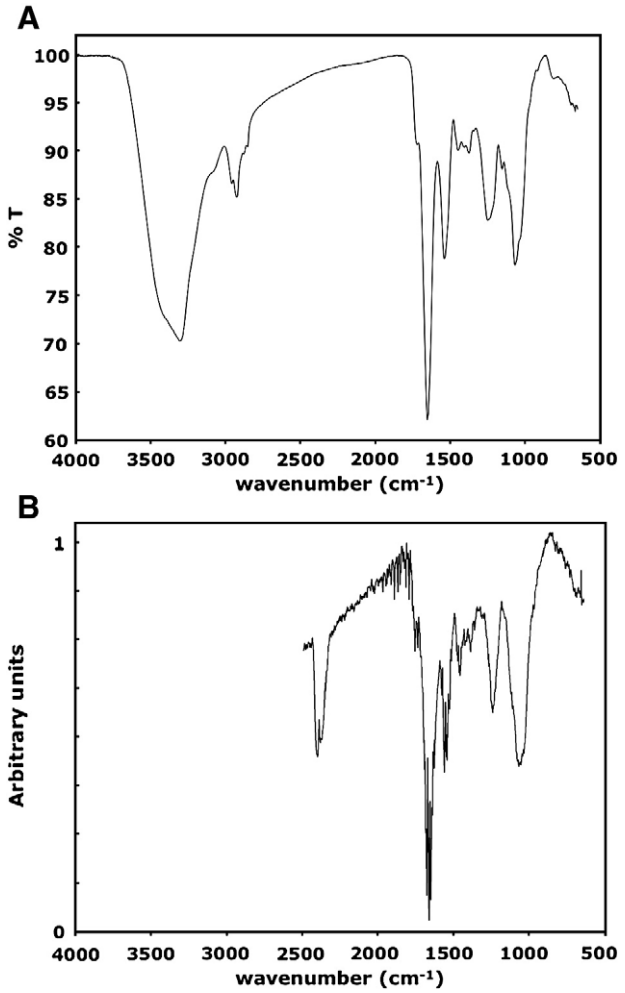

Fig. 2. FTIR spectra of (A) air-dried *Terebellid* burrow wall mucous material (transmission mode microscope-FTIR, this study), and (B) partially-purified and freeze-dried mucous glycoproteins from the brittlestar *Ophiocomina nigra* (zinc-selinide ATR-FTIR, reproduced from Bavington et al., 2004).

those that remain deprotonated over the titration range. A zero proton condition cannot be defined from these data sets, as the mucous material exchanges protons over the entire titration range; instead, charge excess is assigned to zero at pH 4, and all reported charge excess values (and modeled functional group concentrations) are relative to the titration starting point (pH 4). Charge excess is assumed to accumulate with increasing pH by the deprotonation of proton-reactive functional group ligands (L_n) in the form:

$$HL_n^{+1} \leftrightarrow L_n^{-1} + H^+ \quad (2)$$

Discrete ligand models accounting for excess charge by functional group deprotonation were fitted to the data in two ways: (1) using linear programming to optimize ligand concentrations at every possible point in a fixed pK_a interval (in this case, 4 to 10 in 0.2 increments) (Matlab script complements of D. Scott Smith; c.f. Brassard et al., 1990; Cox et al., 1999; Smith et al., 1999; Lalonde et al., 2008, for further details), and (2) using least squares optimization in FITEQL (Westall, 1982) to resolve, for a predetermined number of ligands, pK_a values and ligand concentrations that best describe the excess charge data. In the case of the latter, a three-ligand model adequately described the data ($V(Y) = 3.70 \pm 0.20$ (2 SE)), and a four-ligand model provided no significant improvement. A non-electrostatic model (NEM) was chosen here for simplicity, as only one ionic strength (0.5 M NaCl) was explored, and recent studies have indicated that electrostatic surface field effects on protonation are minimal relative to experimental uncertainties for routine titration of organic materials such as bacterial surfaces (Borrok and Fein, 2005) and humic/fulvic acids (Borrok and Fein, 2004).

Charge excess in the titration, assumed here to arise solely by the deprotonation of organic functional groups in the mucous material, is presented in Fig. 3A. Distinct inflection points are absent in the titration data, consistent with complex organic matter possessing diverse functional groups with pK_a values distributed over the entire titration range. Interestingly, the shape of the charge excess curves mimic those determined for a variety of humic and fulvic substances by Milne et al. (2001). Differences in excess charges between titration replicates represent some degree of irreproducibility, possibly indicating sample heterogeneity. Discrete ligand models fit to the excess charge data are presented as calculated excess charge (solid and stippled lines in Fig. 3A), and as pK_a spectra in Fig. 3B (linear programming optimization) and Fig. 3C (least squares optimization). While the discrete ligand model developed by least squares optimization (Fig. 3C) was constrained to three ligands by the optimization algorithm, the number of ligands in the model developed by linear programming is limited only by the chosen pK_a interval (in this case, 30 ligands, spanning from pK_a 4–10 in increments of 0.2), and a best fit was obtained by a combination of three major ligands and three minor ligands. The three major ligands in this model approximately correspond to the three ligands in the least squares model in terms of pK_a and concentration (see Fig. 3; Table 1). Based on compositional data, FTIR spectra, and analogy in acidity constant with respect to known compounds, the three ligands likely correspond to carboxyl, phosphoryl, and thiol groups, respectively, although, more detailed spectroscopy aimed at determining surface ligand structures would be required for absolute identification (see discussion below). Differences between the two models, namely the presence of "other ligands" beyond the three major ligands identified by both, can be attributed to the fact that the linear programming optimization possesses the freedom to attribute excess charge from what would be restricted to a single ligand in the least squares optimization to multiple ligands in the linear programming optimization, for marginally small increases in the goodness of fit of the model. As both models describe the titration data with little relative error, the supposition of additional ligands by the linear programming optimization is of little benefit. As such, it is presented only for the purposes of comparison to other studies where linear programming optimization was similarly employed.

The model parameters fitted to the titration data are presented in Table 1; both modeling approaches yielded total ligand concentrations in the pK_a 4 to 10 range of approximately 11 mmol per dry gram, with no significant difference in total ligand concentrations between the two models (within experimental uncertainty). This value is relatively high compared to that observed for fulvic substances (7.74 mmol/g, average of 25 fulvic acids, Milne et al. (2001)), humic substances (5.70 mmol/g, average of 24 humic acids, Milne et al. (2001)), and bacterial surfaces (3.2 mmol/g (assuming a dry:wet ratio of 10:1), average of 36 bacterial species, Borrok et al. (2005)) (Fig. 4). It is also significantly higher than values observed for inorganic phases commonly considered to be important sorbents in surface and near-surface environments, such as hydrous ferric oxide (synthetic: 2.42 mmol/g, Smith and Ferris, 2001; natural, 2.16 to 5.44 mmol/g, Lalonde et al., 2007). The elevated surface ligand concentration of the mucous material relative to other organic materials is possibly due to the highly soluble nature and extended fiber conformation of mucin-type materials at circumneutral pH; porcine gastric mucin, an analogous compound often employed for the physiological study of mucus and as a growth substrate for enterobacteria, possesses an extended fibrous structure of 1–2 nm in diameter and approximately 400 nm in length at pH 5–7 (Hong et al., 2005). Such an extended

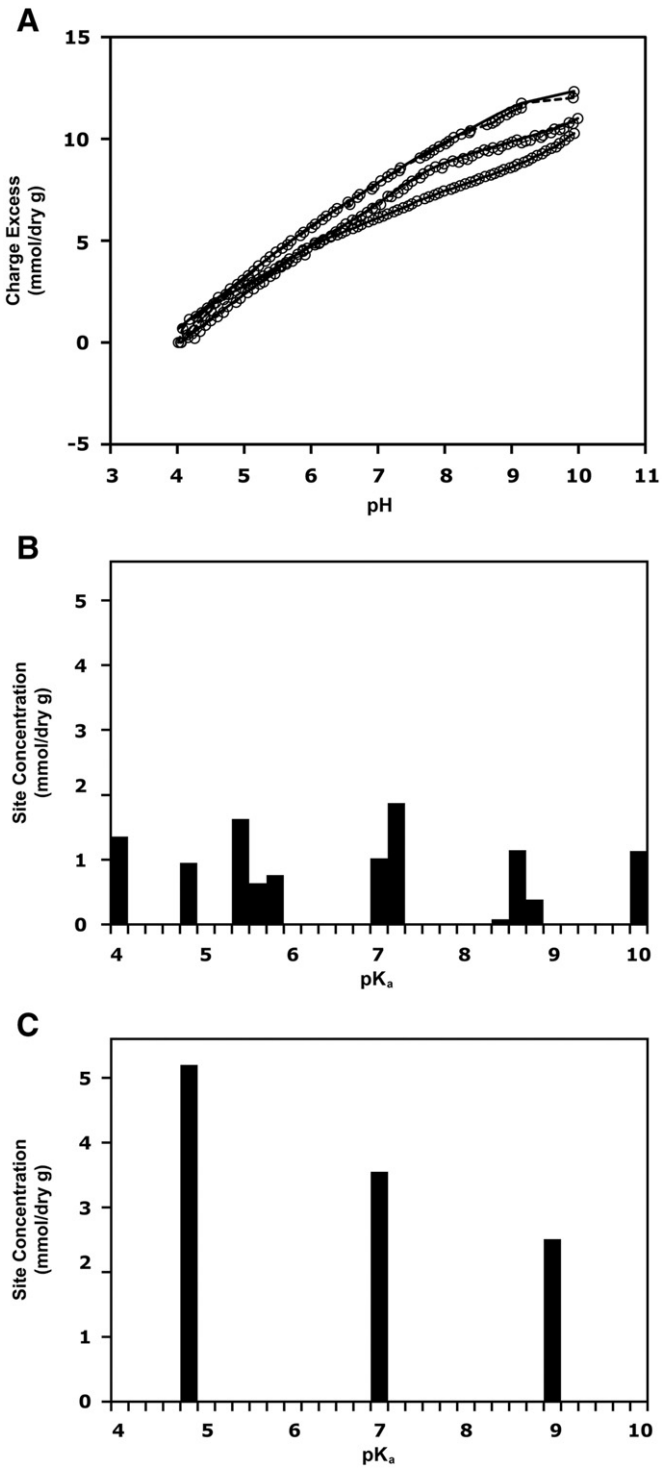

Fig. 3. (A) Excess charge arising as a function of pH during acid-base titration, reflecting progressive deprotonation of organic functional groups comprising the mucous material. Data points represent titration data, while solid and stippled lines represent the model fit excess charge calculated from the discrete ligand models presented in (B) and (C). In (B) and (C), best-fit discrete ligand models obtained by linear programming (B) and least squares (C) optimization represent the set of functional groups, in terms of concentration (*y*-axis) and acidity constant (*x*-axis), that best describe the charge excess data. The least squares optimization was constrained in number of ligands (three) while the linear programming optimization was constrained by pK_a resolution (pK_a values only permitted in increments of 0.2).

conformation may provide proton access to ligands that would otherwise be inaccessible in more aggregated biomolecules. The mucous material possesses an acid-base reactivity (over the pH 4–10 range) that is 1.2 to 3 times that of other forms of natural organic matter (e.g. fulvic, humic, and bacterial organic matter; Fig. 4); clearly, the mucous material possesses the potential, in terms of available reactive ligands, to significantly influence dissolved ion mobility at the organic-water interface. Furthermore, the mucous material exchanges protons over the entire titration range investigated herein (pH 4–10), such that with increasing pH, the proportion of deprotonated ligands that are available to participate in cation adsorption reactions increases steadily with increasing pH. At typical seawater pH (7.4–8.2), approximately half of the inferred ligands should be in an anionic form immediately conducive to metal adsorption. Thus, with respect to both adsorption ligand density and availability, and in terms of reactive components in marine sediment, mucous materials associated to burrowing animals should be considered an important potential sink for metals. We further investigate this potential using batch Cd adsorption experiments, described below.

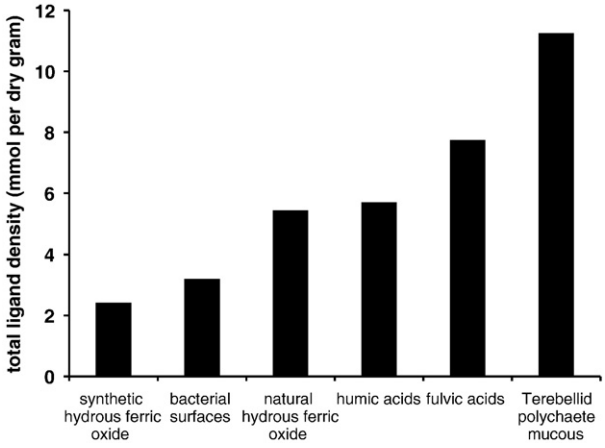

Fig. 4. Comparison of *Terebellid* mucous total ligand density (summed over pH 4–10 range) with other materials considered important adsorbents in natural systems. See text for values and references.

3.3. Cadmium adsorption

In addition to the availability of absorptive ligands in terms of concentration, the stability of surface-complexed metals at each of these ligands also plays a central role in determining partitioning between solid surfaces and the aqueous phase. We evaluated metal-ligand stability constants using Cd for several reasons: (1) Cd remains soluble over the pH range of interest, (2) to facilitate comparison with other metal adsorption studies involving fulvic/humic acids and bacteria; and (3) relevance to near-shore ocean and estuary waters where Cd concentrations may be elevated.

For our experimental conditions (approximating seawater chloride salinity), chemical equilibrium modeling reveals that Cd is present largely as the chloride complexes $CdCl_2$ (aq) and $CdCl^-$, with lesser $CdCl_3^-$ and Cd^{2+} (Fig. 5). In the pH 2–10 working range, these dominant species are largely insensitive to changes in pH, although at alkaline pH the hydrolyzed Cd species $CdOHCl^0$ (aq), and to a lesser extent, $CdOH^+$, and $Cd(OH)_2$ (aq), become important. $Cd(OH)_2$ (s) precipitation was not indicated for any experimental condition. Stability constants from the MINTEQA2 v4.0 database (Allison et al., 1991) for all Cd species displayed in Fig. 5 were included for consideration in modeling of Cd-ligand stability constants, discussed below.

Experimental data for Cd adsorption to worm mucous material is presented in Fig. 6. Cd adsorption generally increases with increasing pH as functional groups progressively deprotonate, however, at low pH some Cd is adsorbed despite the fact that ligands 1–3 are largely protonated below pH 4. For surface complexation modeling of Cd

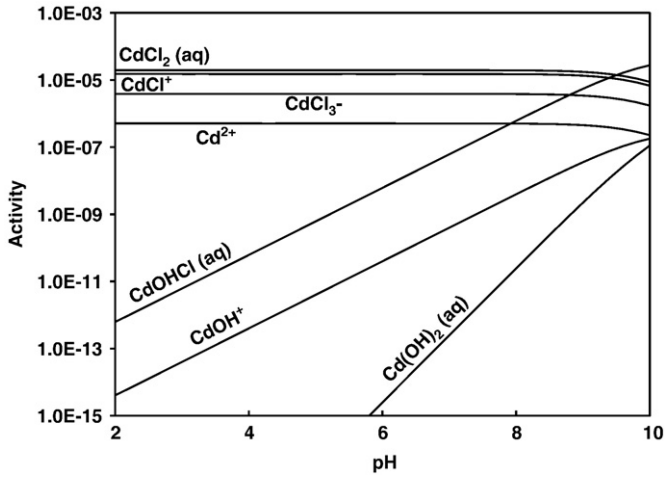

Fig. 5. Aqueous Cd speciation as a function of pH for the Cd adsorption conditions (0.5 M NaCl, 5 ppm Cd, pH 2–10). Cadmium chloride complexes form the dominant species below pH ~ 9. See Methods section for equilibrium modeling details.

adsorption data, Cd-ligand stability constants were defined based on the following hypothesized surface adsorption reactions, for ligands L_1–L_3 identified by least squares optimization of titration data (Table 2):

$$L_n^{-1} + Cd^{2+} \leftrightarrow L_n Cd^{+1} \quad (3)$$

These three reactions alone were insufficient to account for adsorption data at low pH (see below), and at high pH, $CdOHCl^0$ becomes the dominant Cd species; accordingly, two additional reactions were considered in the adsorption models:

$$HL_n + Cd^{2+} \leftrightarrow HL_n Cd^{+2} \quad (4)$$

$$L_n^{-1} + CdOHCl^0 \leftrightarrow L_n CdOHCl^- \quad (5)$$

Reaction (4) involves Cd adsorption to a fully protonated functional group and can account for the observed Cd adsorption at low pH where no ligands are significantly deprotonated, while reaction (5) can account for Cd adsorption at alkaline pH where $CdOHCl^0$ is the most abundant Cd species (as per Fig. 5). Various permutations of possible adsorption reactions were examined for fit to the data using the program FITEQL (Westall, 1982). Table 3 lists the individual models considered, along with best-fit Cd-ligand stability constants and a model variance parameter ($V(Y)$) that provides an indication of goodness-of-fit, with smaller values indicating better agreement between the experimental data and the model.

Models invoking Cd adsorption to only one or two of the three ligands provided relatively poor fits (Table 3), as did models negating the possibility of adsorption to protonated sites (reaction (4)). It can be seen from both model variance parameters and fitted log K values that model fit was insensitive to the particular ligand (HL1, HL2, HL3) chosen as the site for protonated-ligand Cd adsorption (i.e., compare models 10–11, 13–15); this is due to high similarity in ligand concentrations and protonation states at low pH ranges where HL_xCd^{2+} surface complexation is most important to the model fit. Model fit was similarly insensitive to choice of ligands forming complexes with $CdOHCl^0$ because this Cd species has little effect on model fit until pH >9 where its concentration becomes important. While consideration of Cd adsorption in the form of $CdOHCl^0$ logically follows from its increasing importance at alkaline pH (see Fig. 5), the consideration of Cd adsorption in the form of Cd^{2+}, to both protonated and deprotonated sites, is less obvious. Cd^{2+} should, with its smaller radius and greater charge, be the most reactive of the Cd species under consideration, and indeed, previous work indicates that the reactivity

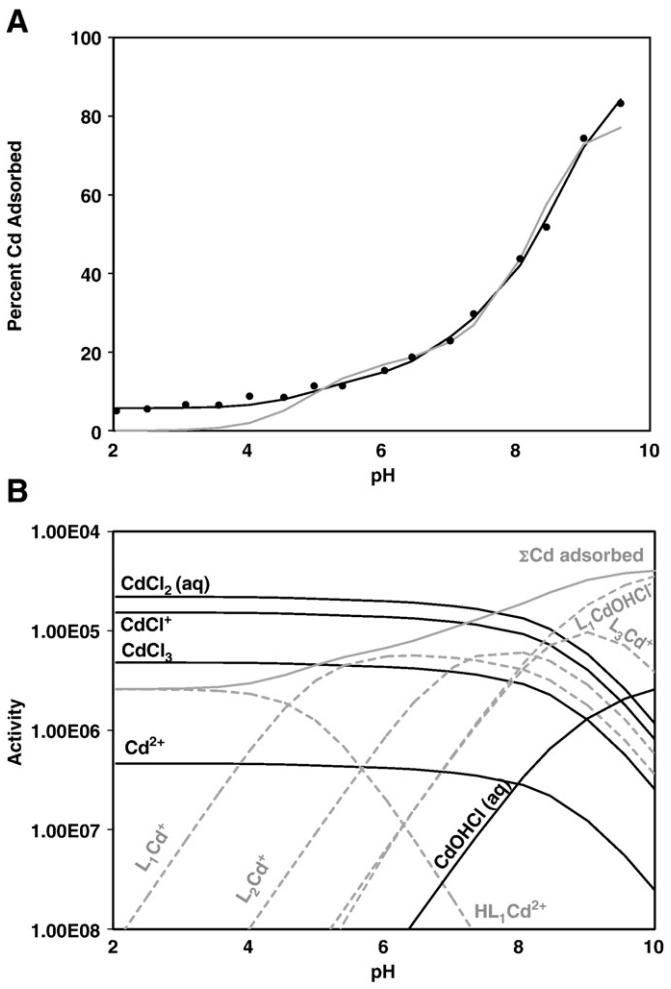

Fig. 6. (A) Cd adsorption data (points) as a function of pH for 5 ppm Cd solutions with 1.0 g/L of mucous material. Two non-electrostatic Cd surface complexation models are presented: Cd^{2+} adsorption to deprotonated ligands L1–L3 only (Table 3, model 12; grey line), and the same with the inclusion of reactions (4) and (5) (Table 3, model 16; black line). Best-fit is achieved when reactions (4) and (5) are considered, better accounting for adsorption at the low and high pH extremes, respectively, although the importance of reaction (5) is relatively small and unsupported (see text). (B) Cd speciation calculated for the best fitting model (Table 3, model 16; black line in (A)) as a function of pH in the Cd adsorption experimental conditions. Aqueous species are presented as black solid lines, adsorbed species as grey dotted lines, and the total Cd adsorbed as a solid grey line.

of cadmium–chlorine complexes appears negligible compared to Cd^{2+} (Voegelin et al., 2001; Temminghoff et al., 1995). However, it must be noted that due to relatively unchanging speciation of dissolved cadmium over the experimental pH range (2–10), adsorption reactions involving Cd species other than Cd^{2+}, such as $CdCl^+$, $CdCl_2$ (aq), and $CdCl_3^-$, while less likely to be important, cannot be ruled out by the adsorption data alone.

Best fit to total Cd adsorbed is achieved when all three ligands are modeled as participating in Cd adsorption, and when reactions (4) and (5) are included (models 16–18, essentially identical in goodness-of-fit). Cd adsorption calculated for one of these models (model 16, black line) is presented alongside the experimental data in Fig. 6A, accompanied by calculated Cd speciation over the experimental pH range (Fig. 6B). Also included in Fig. 6A is model 12 (grey line), where only Cd^{2+} adsorption to the three deprotonated ligands are considered. The increase in model goodness-of-fit resulting from the consideration of reaction (4) and (5) is readily apparent, where HL_1Cd^{2+} better accounts for adsorption at low pH, and $L_1CdOHCl^-$ provides slightly increased fit at high pH, respectively. The increase in model goodness-of-fit by consideration of reaction (5) is relatively minor (compare

Table 2
Parameters obtained from best-fit non-electrostatic proton adsorption models of titration data. For the purposes of comparison, ligands in the linear programming model with pK_a values below 5 or above 9 were classified as "other ligands". These ligands, while always indicated by linear programming, were inconsistent in pK_a between independent titrations. Uncertainties represent 2SE calculated from independent modeling of titration triplicates.

	pK_a			Concentration (mmol/g)				Total
	Site 1	Site 2	Site 3	Site 1	Site 2	Site 3	Other sites	
Linear programming (MATLAB 7)	5.57 ± 0.23	7.14 ± 0.06	8.65 ± 0.14	3.01 ± 0.61	3.07 ± 0.70	1.65 ± 0.95	3.26 ± 0.92	10.99 ± 3.18
Sum of squares (FITEQL 4.0)	4.89 ± 0.18	6.93 ± 0.26	8.98 ± 0.50	5.20 ± 0.23	3.55 ± 0.88	2.51 ± 0.68	n/a	11.26 ± 1.79

models 13–15 with 16–18); this is attributable to the fact that reaction (5) is important only at the alkaline extreme of the adsorption experiments, and as such, support for it in this dataset is relatively weak, resting on a single data point. While $CdOHCl^0$ adsorption could be ignored for the modeling of most natural waters (i.e., pH < 9) without consequence (Table 3), it is included here for the consideration of future studies examining Cd adsorption at more alkaline or saline conditions where $CdOHCl^0$ is the dominant Cd species. At low pH, it should be noted that some adsorption may be due to functional groups undetected by titration that continue to exchange protons and metals at low pH; such appears to be the case with fulvic substances (Saar and Weber, 1979), humic substances (Liu and Gonzalez, 2000) and bacteria (Fein et al., 2005).

Although certain assignment of specific ligand identities (such as the carboxyl, phosphoryl, thiol, amino, and hydroxyl functional groups typical of organic matter) is not possible without additional spectroscopic evidence, assignment based on acidity constants alone, in a manner similar to Fein et al. (1997), would indicate that ligands 1 and 2 represent carboxyl and phosphoryl groups, respectively. Best-fit Cd-ligand stability constants (log *K* values; model 16) for these ligands are 2.19 and 3.86, surprisingly comparable to some ligands of similar pK_a that have been indicated for a range of bacterial consortia (log *K* values of 2.7 and 3.95; sites 2 and 3, Borrok et al., 2004). With this tentative ligand assignment, the adsorption of Cd^{2+} as a function of pH onto deprotonated ligands L1 and L2 (Fig. 6B) parallels observations from X-ray adsorption fine-edge spectroscopy of Cd adsorption to *Bacillus subtilis* cell walls (Boyanov et al., 2003) in that Cd adsorption occurs predominately to carboxyl ligands at pH ranges between 5–7, with smaller contribution from a possible Cd-phosphoryl complex at higher pH (> 7.8).

Table 3
Cd adsorption models based on adsorption data (points in Fig. 5) and the three proton-reactive ligands (L1, L2, L3) indicated by titration. HL1, HL2, and HL3 correspond to the same ligands in protonated form. Fitted model parameters (log *K*) are provided in order of the Cd-complexing ligands under consideration (first column), along with an indication of model fit (the FITEQL variance function *V*(*Y*)), where smaller values indicate better fit to the data.

Model	Cd-complexing ligands	log *K*					*V*(*Y*)
		$L_xCdOHCl^*$	HL_xCd^{2+}	CdL1	CdL2	CdL3	
1	L1 only			−1.65			54.08
2	L2 only				−3.17		24.93
3	L3 only					−4.17	17.66
4	L1 and HL1		1.91	−1.66			57.51
5	L2 and HL2		2.48		3.18		22.28
6	L3 and HL3		2.86			−4.27	4.54
7	L1 and L2			−2.44	−3.22		25.47
8	L2 and L3				−3.52	−4.47	9.28
9	L1 and L3			−2.04		−4.36	3.08
10	HL1, L1, L3		2.24	−2.07		−4.35	1.22
11	HL3, L1, L3		2.56	−2.21		−4.35	1.22
12	L1–L3			−2.07	−4.41	−4.38	3.24
13	HL1, L1–L3		2.27	−2.16	−4.10	−4.40	0.99
14	HL2, L1–L3		2.44	−2.34	−3.95	−4.40	0.99
15	HL3, L1–L3		2.59	−2.34	−4.10	−4.39	0.99
16	HL1, HL1, L1–L3	−9.62	2.28	−2.19	−3.86	−4.88	0.30
17	HL2, HL2, L1–L3	−11.49	2.45	−2.41	−3.74	−4.89	0.30
18	HL3, HL3, L1–L3	−13.39	2.60	−2.41	−3.86	−4.57	0.30

The third site (L3) possesses the highest Cd-ligand stability constant. Strong Cd adsorption in this pH range is consistent with the presence of highly-chalcophile thiol functional groups as indicated by infrared spectroscopy (discussed above). The assignment of the highly Cd-reactive thiol functional groups for ligand 3, in lieu of other possible organic ligands for this acidity range (e.g., amino, hydroxyl), is preferred as the latter have not been reported to possess strong affinity for Cd, whereas Cd adsorption to thiol groups is strong (log *K* values of 8.8 and 4.8 for 3-mercaptopropionic acid Cd^{2+} -monothio and -diothio complexes, respectively; Vairavamurthy et al., 2000). Indeed, the high thiol functional group content of mucus and mucin-type glycoproteins has been long known, and has been implicated in the strong adhesivity of these materials by enhanced disulfide cross-linking ability (e.g., Leitner et al., 2003).

It appears that mucous materials such as the *Thelepus* mucus studied herein possess strong affinities for chalcophile elements such as Cd, potentially as a consequence of their "sticky" nature conferred by the presence of abundant thiol groups and thiol-rich cysteine residues. It is possible that mucous materials possess, or once possessed, a dual function, one being physical protection in the form of adhesion and resistance to desiccation, and the other being chemical, acting as a nutrient sieve that focuses metals and nutrients for the organism's benefit, or perhaps the benefit of the microbial colonies that typically accompany the linings of burrowing organisms in a symbiotic fashion (e.g., Aller and Aller, 1986). Given their small size, dense surface ligand concentrations, and pervasive occurrence across the animal kingdom, mucus secretions comprised of mucin-type glycoproteins hold a vast potential with respect to metal sequestration budgets in estuarine settings. Further work quantitatively exploring the distribution and abundance of such mucous materials in estuarine sediments will enable a better understanding of the overall importance of such materials in the sequestration of dissolved metals and contaminants.

4. Conclusion

It was determined that the mucous material produced during bioturbation by *Thelepus crispus* worms consists of a mucin-type glycoprotein that is homologous to other marine animal mucus secretions (e.g., those of echinoderms), and is likely representative of mucous secretions throughout the marine worm community. Acid-base titrations revealed that the mucous material possesses unusually high proton reactivities, on the order of 11 mmol per dry gram summed over pH 4 to 10, with proton-exchanging ligands distributed approximately equally across the titration range. Discrete ligand modeling indicated that three ligands are sufficient to accurately describe proton adsorption across the titration range, and when considered in combination with FTIR and compositional data, indicate the presence of abundant proton-exchanging carboxyl, phosphoryl, and thiol functional groups. Cd adsorption experiments indicate strong adsorption of Cd to worm mucous material, with Cd-ligand stability constants comparable to those determined for bacterial surfaces. While it is possible that worm mucous linings play some physiological role as ion-selective sieves, it is clear that they serve as efficient sorbents for chalcophile elements such as Cd, potentially due

in part to high thiol functional group content. Based on these findings, the mucous secretions produced by burrowing marine organisms should not be overlooked when evaluating seawater metal partitioning at the sediment-water interface.

Acknowledgments

The authors would like to thank Ron Koss for marine aquarium access and worm incubating assistance, and Tara Macdonald for help with worm species identification. Constructive suggestions and reviews by Editor Jeremy Fein and two anonymous reviewers improved the manuscript significantly, and are greatly appreciated. This work was supported by National Science and Engineering Research Council (NSERC) and Alberta Ingenuity Student Awards to SL and LD, and NSERC Discovery Grants to KK, MG, and GP.

References

Aller, J.Y., Aller, R.C., 1986. Evidence for localized enhancement of biological activity associated with tube and burrow structures in deep-sea sediments at the HEBBLE site, western North Atlantic. Deep Sea Res. Part A 33 (6A), 755–790.

Allison, J.D., Brown, D.S., Novo-Gradac, K.J., 1991. MINTEQA2/PRODEFA2, A geochemical assessment model for environmental systems: Ver. 3.0 Users manual. Athens, GE, USA: US EPA.

Bavington, C.D., Lever, R., Mulloy, B., Grundy, M.M., Page, C.P., Richardson, N.V., McKenzie, J.D., 2004. Anti-adhesive glycoproteins in echinoderm mucus secretions. Comp. Biochem. Physiol. Part B: Biochem. Mol. Biol. 138 (4), 607–617.

Benoit, G., Oktay-Marshall, S.D., Cantu, A., Hood, E.M., Coleman, C.H., Corapcioglu, M.O., Santaschi, P.H., 1994. Partitioning of Cu, Pb, Ag, Zn, Fe, Al, and Mn between filter-retained particles, colloids, and solution in six Texas estuaries. Mar. Chem. 45 (4), 307–336.

Borrok, D.M., Fein, J.B., 2004. Distribution of protons and Cd between bacterial surfaces and dissolved humic substances determined through chemical equilibrium modeling. Geochim. Cosmochim. Acta 68 (14), 3043–3052.

Borrok, D.M., Fein, J.B., 2005. The impact of ionic strength on the adsorption of protons, Pb, Cd, and Sr onto the surfaces of Gram negative bacteria: testing non-electrostatic, diffuse, and triple-layer models. J. Colloid Interface Sci. 286 (1), 110–126.

Borrok, D.M., Turner, B.F., Fein, J.B., 2005. A universal surface complexation framework for modeling proton binding onto bacterial surfaces in geological settings. Am. J. Sci. 305 (6–8), 826–853.

Boyanov, M.I., Kelly, S.D., Kemner, K.M., Bunker, B.A., Fein, J.B., Fowle, D.A., 2003. Adsorption of cadmium to *Bacillus subtilis* bacterial cell walls: A pH-dependent X-ray absorption fine structure spectroscopy study. Geochim. Cosmochim. Acta 67 (18), 3299–3311.

Brandenburg, K., Seydel, U., 1996. Fourier transform infrared spectroscopy of cell surface polysaccharides. In: Mantsch, H.H., Chapman, D. (Eds.), Infrared Spectroscopy of Biomolecules. Wiley-Liss, New York, pp. 203–237.

Brassard, P., Kramer, J.R., Collins, P.V., 1990. Binding site analysis using linear programming. Environ. Sci. Technol. 24 (2), 195–201.

Bryan, G.W., Hummerstone, L.G., 1973. Adaptation of the polychaete Nereis diversicolor to estuarine sediments containing high concentrations of zinc and cadmium. J. Mar. Biol. Assoc. U.K. 53 (4), 839–857.

Bryan, G.W., Langston, W.J., 1992. Bioavailability, accumulation and effects of heavy metals in sediments with special reference to United Kingdom estuaries: a review. Environ. Pollut. 76 (2), 89–131.

Bryan, G.W., Langston, W.J., Hummerstone, L.G., Burt, G.R., Ho, Y.B., 1983. An assessment of the gastropod, Littorina littorea, as an indicator of heavy-metal contamination in United Kingdom Estuaries. J. Mar. Biol. Assoc. U.K. 63 (2), 327–345.

Chiffoleau, J.F., Cossa, D., Auger, D., Truquet, I., 1994. Trace metal distribution, partition and fluxes in the Seine Estuary (France) in low discharge regime. Mar. Chem. 47 (2), 145–158.

Cox, J.S., Smith, D.S., Warren, L.A., Ferris, F.G., 1999. Characterizing heterogeneous bacterial surface functional groups using discrete affinity spectra for proton binding. Environ. Sci. Technol. 33 (24), 4514–4521.

Fein, J.B., Boily, J.-F., Yee, N., Gorman-Lewis, D., Turner, B.F., 2005. Potentiometric titrations of *Bacillus subtilis* cells to low pH and a comparison of modeling approaches. Geochim. Cosmochim. Acta 69 (5), 1123–1132.

Fein, J.B., Daughney, C.J., Yee, N., Davis, T.A., 1997. A chemical equilibrium model for metal adsorption onto bacterial surfaces. Geochim. Cosmochim. Acta 61 (16), 3319–3328.

Gustafsson, J.P. (2000) Visual Minteq [www document]. URL http://www.lwr.kth.se/English/OurSoftware/vminteq/ (verified 25 October 2009).

Hong, Z., Chasan, B., Bansil, R., Turner, B.F., Bhaskar, K.R., 2005. Atomic force microscopy reveals aggregation of gastric mucin at low pH. Biomacromolecules 6 (6), 3458–3466.

Konhauser, K.O., 2007. Introduction to Geomicrobiology. Blackwell publishing, Oxford, UK.

Lalonde, S.V., Amskold, L., Mcdermott, T.R., Inskeep, W.P., Konhauser, K.O., 2007. Chemical reactivity of microbe and mineral surfaces in hydrous ferric oxide depositing hydrothermal springs. Geobiology 5 (3), 219–234.

Lalonde, S.V., Smith, D.S., Owttrim, G.W., Konhauser, K.O., 2008. Acid–base properties of cyanobacterial surfaces I: Influences of growth phase and nitrogen metabolism on cell surface reactivity. Geochim. Cosmochim. Acta 72 (5), 1257–1268.

Lang, T., Hansson, G.C., Samuelsson, T., 2007. Gel-forming mucins appeared early in metazoan evolution. Proc. Nat. Acad. Sci. 104 (41), 16209–16214.

Leitner, V.M., Walker, G.F., Bernkop-Schnürch, A., 2003. Thiolated polymers: evidence for the formation of disulphide bonds with mucus glycoproteins. Eur. J. Pharm. Biopharm. 56 (2), 207–214.

Liu, A., Gonzalez, R.D., 2000. Modeling adsorption of copper (II), cadmium (II) and lead (II) on purified humic acid. Langmuir 16 (8), 3902–3909.

Luoma, S.N., Van Geen, A., Lee, B.G., Cloern, J.E., 1998. Metal uptake by phytoplankton during a bloom in South San Francisco Bay: Implications for metal cycling in Estuaries. Limnol. Oceanogr. 43 (5), 1007–1016.

Maynard, L.A., Loosli, J.K., 1969. Animal Nutrition. 6th Ed., McGraw-Hill, New York, USA.

Millward, G.E., Glegg, G.A., 1997. Fluxes and retention of trace metals in the Humber Estuary. Estuarine Coastal Shelf Sci. 44 (Supp. A), 97–105.

Milne, C.J., Kinniburgh, D.G., Tipping, E., 2001. Generic NICA-Donnan model parameters for proton binding by humic substances. Environ. Sci. Technol. 35 (10), 2049–2059.

Over, D.J., 1988. Lingulid brachiopods and Lingulichnus from a Silurian shelf-slope carbonate sequence, Delorme Group, Mackenzie Mountains, Norwest Territories. Can. J. Earth Sci. 25 (3), 465–471.

Pettit, L.D., Sukhno, I., Buzko, V., 2006. Ionic Strength Corrections for Stability Constants using Specific Interaction Theory. Ver. 2.0. York. IUPAC-Academic Software, UK.

Rouse, G.W., Fauchald, K., 1997. Cladistics and polychaetes. Zool. Scr. 26 (2), 139–204.

Saar, R.A., Weber, J.H., 1979. Complexation of cadmium (II) with water-and soil-derived fulvic acids: effect of pH and fulvic acid concentration. Can. J. Chem. 57 (11), 1263–1268.

Smith, D.S., Adams, N.W.H., Kramer, J.R., 1999. Resolving uncertainty in chemical speciation determinations. Geochim. Cosmochim. Acta 63 (19–20), 3337–3347.

Smith, D.S., Ferris, F.G., 2001. Proton binding by hydrous ferric oxide and aluminum oxide surfaces interpreted using fully optimized continuous pK_a spectra. Environ. Sci. Technol. 35 (23), 4637–4642.

Temminghoff, E.J.M., Van Der Zee, S.E.A.T.M., De Haan, F.A.M., 1995. Speciation and calcium competition effects on cadmium sorption by sandy soil at various pHs. Eur. J. Soil Sci. 46, 649–655.

Vairavamurthy, M.A., Goldenburg, W.S., Ouyang, S., Khalid, S., 2000. The interaction of hydrophilic thiols with cadmium: investigation with a simple model, 3-mercapto-propionic acid. Mar. Chem. 70, 181–189.

Voegelin, A., Vulava, V.M., Kretzschmar, R., 2001. Reaction-based model describing competitive sorption and transport of Cd, Zn, and Ni in an acidic soil. Environ. Sci. Technol. 35 (8), 1651–1657.

Westall, J.C., 1982. FITEQL: A computer program for determination of chemical equilibrium constants from experimental data. Version 4.0, Dept. Chem., Oregon St. Univ., Corvallis, OR, USA.

Zorn, M.E., Muehlenbachs, K., Gingras, M.K., Konhauser, K.O., Pemberton, S.G., Evoy, R., 2007. Stable isotopic analysis reveals evidence for groundwater-sediment-animal interactions in a marginal-marine setting. Palaios 22 (5), 546–553.